INTERNATIONAL JOURNAL FOR NUMERICAL METHODS IN FLUIDS
Int. J. Numer. Meth. Fluids 2005; **47**:739–758
Published online 27 January 2005 in Wiley InterScience (www.interscience.wiley.com). DOI: 10.1002/fld.913

A predictor–corrector formulation for rigorous streamline simulation‡

Michael J. King[1,*,†], Ichiro Osako[2] and Akhil Datta-Gupta[2]

[1] *DPNW, EPTG, BP America, Inc., Houston, TX 77079, U.S.A.*
[2] *Department of Petroleum Engineering, Texas A&M University, College Station, TX 77843, U.S.A.*

SUMMARY

Streamline simulators have received increased attention in the petroleum industry because of their ability to effectively handle multimillion cell detailed geologic models and large simulation models. The efficiency of streamline simulation has relied primarily on their ability to take large time steps with fewer pressure solutions within an IMPES formulation. However, unlike conventional finite difference simulators, no clear guidelines have been available for the choice of time step for pressure and velocity updates. This has remained largely an uncontrolled approximation, either managed by engineering judgment, or by potentially time-consuming time step size sensitivity studies early in a project. This is clearly related to the lack of theoretical understanding of numerical stability and convergence for this solution method. Our results demonstrate a new ability to predict numerical stability for streamline simulation. The analysis of numerical convergence is beyond our current scope. Clearly, both stability and convergence are required for numerical solutions.

We will review the predictor–corrector streamline formulation recently introduced (*SPE 79688, presented at the SPE Reservoir Simulation Symposium*, Houston, TX, 3–5 February 2003). This formulation includes the treatment of transverse flux between streamlines, and for the first time provides a rigorous foundation for discussions of numerical stability. We extend those discussions to include the treatment of capillarity and of gravity. In all instances, we will recognize the limits of stability of the calculations through the use of a CFL number, or in the instance of capillarity, a diffusion number. Although the worked examples will all utilize explicit numerical techniques, in most instances, the use of implicit techniques will be obvious.

We demonstrate the validity and utility of our approach using a series of numerical experiments in homogeneous and heterogeneous $\frac{1}{4}$ five-spot patterns at various mobility ratios. For the discussions of capillarity and of gravity we also provide one-dimensional calculations to better understand our options for their treatment using operator splitting. For these numerical experiments, we pay particular attention to favourable mobility ratio displacements, as they are known to be challenging to streamline simulation. Our results clearly demonstrate the impact of the transverse flux correction on the accuracy of the solution and on the appropriate choice of time step, across a range of mobility ratios. The proposed approach eliminates much of the subjectivity associated with time step selection in streamline

*Correspondence to: Michael J. King, DPNW, EPTG, BP America, Inc., Houston, TX 77079, U.S.A.
†E-mail: KingMJ3@bp.com
‡Presented at the 8th Oxford Institute of Computational Fluid Dynamics Conference Oxford University, Oxford, England, 29 March–1 April 2004.

Received 27 April 2004
Revised 15 December 2004
Accepted 16 December 2004

simulation, and provides a basis for automatic control of pressure time step within full field streamline applications. Copyright © 2005 John Wiley & Sons, Ltd.

KEY WORDS: streamlines; time of flight; finite difference simulation; porous media

1. INTRODUCTION

Streamline simulation has developed rapidly over the last ten years within the oil industry [1–9]. Unlike the earlier streamtube calculations, which date back to the 1930s, streamline simulators have dispensed with the explicit construction of volume elements (the tubes) and replaced them with calculations along lines. Each line may be thought of as tracing out the centre of a streamtube, with the velocity obtained from a numerical finite difference calculation. In contrast, within a streamtube, fluid velocity is obtained from the volumetric flux per unit area, where the area must be calculated explicitly as part of the streamtube construction. With streamlines the geometry is implicit, making it simple to perform calculations in three dimensions. To leading order, the streamline simulation appears as a sum of one-dimensional simulations, and so calculations in one, two or three dimensions are essentially equivalent. It is this ease of formulation which has transformed the class of problems which we can study with streamline simulation. Where streamtube calculations emphasized two-dimensional sweep and pattern floods, streamline simulation has been applied to the full range of multiphase and multi-component physical and chemical processes in three dimensions [10, 11].

For convection driven processes, streamline simulation has a tremendous advantage over conventional finite difference simulation. Transport along each line may be solved by appropriate one-dimensional numerical methods. For multiphase (black oil) simulation, these may be either Lagrangian or Eulerian—both approaches have proven effective. The Lagrangian discretization [12] has no obvious time step limitation. The Eulerian calculations along each line are de-coupled, and so each may be performed optimally. Both explicit and implicit Eulerian techniques have been used. Only Eulerian methods have been successfully applied for multi-component systems because of the difficulty of formulating an appropriate Lagrangian approach.

Irrespective of the numerical techniques used to solve transport along streamlines (Lagrangian or Eulerian, explicit or implicit) streamline simulation is a large time step IMPES calculation, with the 'time step' controlling the frequency of pressure and velocity updates (Figure 1). Until the recent work which examined the impact of transverse flux during a time step [1], there have been no numerical controls on time step size. Instead time stepping has been decided by engineering pre-studies or other heuristic approaches. We will review the treatment of transverse flux in the next section.

This flow chart also emphasizes that the streamline simulator is a hybrid. Portions of the calculation occur on an underlying fixed spatial grid and others occur on the lines. At each time step of the simulator, a numerical calculation is performed for pressures and phase velocities. Trajectories are traced along the total fluid velocity (oil + water + gas) to determine the streamlines. Streamlines are considered to be fixed during a time step. The saturation (or composition) evolution takes several steps. Saturations are sampled onto the streamlines, they are then transported along streamlines using appropriate one-dimensional numerical techniques, and they are then re-sampled or averaged onto the grid. The result is a non-conservative

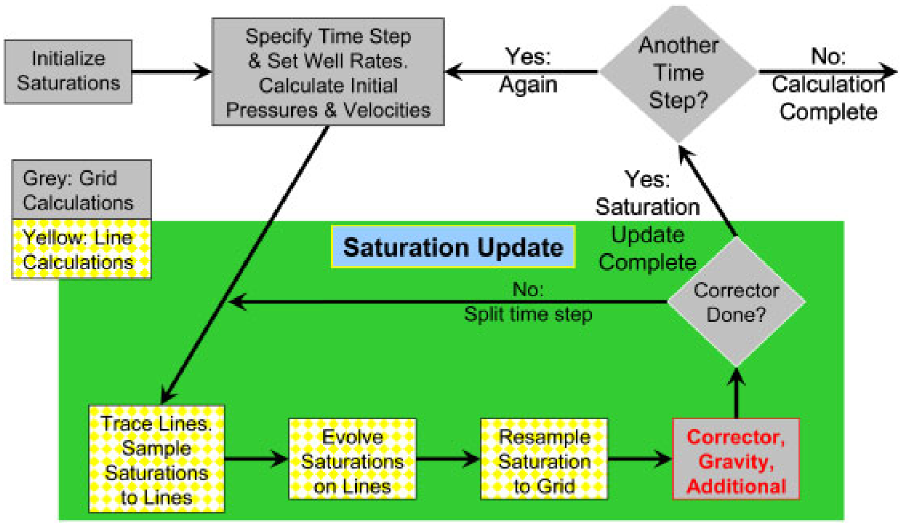

Figure 1. Streamline simulation IMPES formulation.

scheme; re-sampling of saturation introduces mass balance errors. When handled badly, these have been reported to be as large as 30% [13].

Streamline-based computation has made it extremely easy to represent longitudinal transport. It is less obvious how to represent gravity segregation, capillarity and diffusion, and unsteady state velocity effects, all of which act transverse to the streamlines. Transverse mechanisms are resolved using operator splitting techniques. In this diagram of the simulator, the operator splitting occurs at the end of the time step. However, if necessary, the streamline time step may be split into several subsidiary time steps, depending upon the requirements of the transverse mechanisms. We will examine this in more detail in our discussion of operator splitting.

It is interesting to compare the treatment of these transverse mechanisms in streamtube simulation, as compared to streamline simulation. One may consider the streamtubes as defining curvilinear control volumes for a numerical grid. On this grid, we may use any of our numerical techniques to represent either longitudinal or transverse flux. Although the longitudinal flux is, by construction, the larger, the transverse flux is not neglected. In contrast, the lack of explicit volume elements for streamline simulation makes the representation of transverse mechanisms on the streamlines problematic. When we review the streamline formulation we will introduce co-ordinates along and transverse to the streamlines. Longitudinal processes will be easy to represent. More subtle is the issue of transverse flux. The streamline formulation makes it extremely easy to generate finite difference equations for transport along streamlines, but the transverse flux is difficult to represent. This can be seen in Figure 2, where three convecting points that are immediately adjacent across three streamlines diverge in space after passing a stagnation point.

With τ representing a co-ordinate along the streamline, and ψ a transverse co-ordinate, we see that the longitudinal spatial derivative $(\partial/\partial\tau)_\psi$ along each streamline is well defined, while the transverse derivative, $(\partial/\partial\psi)_\tau$, is singular. Although the transformation from (x, y, z) to longitudinal and transverse co-ordinates will have other advantages in our formulation and numerical methods, they do not provide an effective three-dimensional co-ordinate system.

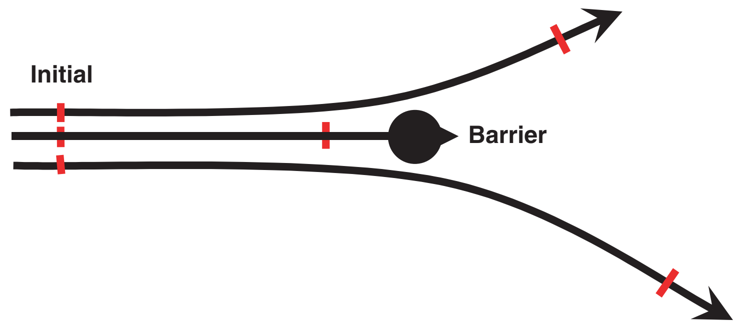

Figure 2. Flow past a stagnation point.

Let us now summarize the attributes of a three-dimensional streamline simulator.

- Streamlines are calculated in three dimensions.
  - Pressures and velocities are obtained from the numerical solution of the pressure equation. As a result they are as flexible in the treatment of spatial heterogeneity and source and sink terms as a conventional finite difference calculation.
  - The streamlines are traced following the total velocity. Transverse phase flux, e.g., gravity segregation or capillary driven flow must be modelled separately. The streamlines themselves are traced across cells using the Pollock [14] algorithm, as generalized by King and Datta-Gupta [9, 15] for corner-point cells and for faulted grids. Streamlines across unstructured grids have also been studied [16, 17].
  - One-dimensional numerical techniques are used to solve for transport along each streamline. Both Eulerian and Lagrangian techniques have been used for black oil. Eulerian methods are used for compositional simulation.
- Pressures and velocities are updated during the calculation
  - Calculations utilize the underlying spatial grid.
  - Studies are not restricted to steady state results, but are instead large time step IMPES calculations.
  - At each time step, saturations are re-sampled introducing potential mass balance errors, and to some extent, re-introducing numerical dispersion.
- Operator Splitting is used to combine mechanisms
  - Gravity and compressibility are included routinely in the existing commercial streamline codes.
  - Capillarity has been included within research codes, but it is not yet in production mode in the commercial simulators.
  - Transverse flux will be managed using this same operator splitting formulation.
  - A CFL construction should be performed to control time stepping for the operator splitting step, as will be discussed in this paper.
- Appropriate allocation of flux to lines
  - The mapping of saturations from lines to cells requires that the volume elements associated with streamlines are calculated appropriately. This is intimately related to flux, and the co-ordinate transformation which underlies the streamline formulation, as will be discussed in the next section.

- Streamline simulation is not...
  - Streamtube simulation. Streamtubes require the construction of explicit volume elements. The velocity of fluid down a streamtube is given by the volumetric flux per unit area. In contrast, for streamlines, the velocity is calculated numerically and the area is obtained implicitly, as the volumetric flux per unit velocity.
  - Front tracking simulation. There are no moving elements corresponding to fronts or to saturation contours. Instead, saturations are interpolated between streamlines in three dimensions at the end of each time step. The resulting saturations may not be mass conserving, and may also have re-introduced numerical dispersion.
  - Restricted to steady state or incompressible flow. However, the usual derivation of the time of flight formulation for streamline simulation is for steady state incompressible flow, which may confuse the unwary reader.

2. STREAMLINE TIME OF FLIGHT FORMULATION

The time of flight formulation [6, 9] is not strictly necessary to construct a streamline simulator. However, it does provide a formal derivation for the approaches used. Especially as these become more problematic, e.g., for compressible fluids, for unsteady state effects, and for multi-component problems, this formulation guides us to an appropriate implementation.

Let us examine the simplest flow equations that demonstrate the time of flight formulation—that of two phase incompressible steady state Darcy flow in a porous media. The equations for waterflood are the saturation evolution equation and the equation for incompressible flow. The latter follows from the mass (or volume) conservation of water plus oil.

$$\phi \frac{\partial S_{\mathrm{w}}}{\partial t} + \nabla \cdot (\mathbf{u} F_{\mathrm{w}}) = 0 \tag{1}$$

$$\nabla \cdot \mathbf{u} = 0 \tag{2}$$

The total fluid Darcy velocity is aligned with the local pressure gradient.

$$\mathbf{u} = -\lambda_{\mathrm{t}} \nabla P \tag{3}$$

The coefficient between $\mathbf{u}$ and ∇P is the total mobility, which depends upon the permeability of the medium, and the relative permeabilities and viscosities of the fluid phases.

$$\lambda_{\mathrm{t}} = k \cdot \left(\frac{k_{\mathrm{rw}}}{\mu_{\mathrm{w}}} + \frac{k_{\mathrm{ro}}}{\mu_{\mathrm{o}}} \right) \tag{4}$$

The fractional flow of water is equal to the ratio of water phase and total mobilities.

$$F_{\mathrm{w}} = \frac{\lambda_{\mathrm{w}}}{\lambda_{\mathrm{t}}} = \left(\frac{k_{\mathrm{rw}}}{\mu_{\mathrm{w}}} \right) \Big/ \left(\frac{k_{\mathrm{rw}}}{\mu_{\mathrm{w}}} + \frac{k_{\mathrm{ro}}}{\mu_{\mathrm{o}}} \right) \tag{5}$$

The permeability depends upon position, $k(\mathbf{x})$, whilst the relative permeabilities depend upon the phase saturation and also the rock type.

In the examples to be shown, we will use quadratic relative permeabilities for each phase. The mobility ratio, M, is defined as the ratio of the mobility of water at the residual oil saturation to the mobility of oil at the irreducible water saturation. For simplicity of exposition, the endpoint saturations will be scaled to [0,1], e.g. $S_{\mathrm{orw}}=0$, $S_{\mathrm{wirr}}=0$.

$$\begin{aligned} k_{\mathrm{ro}} &= \left(\frac{1-S_{\mathrm{orw}}-S_{\mathrm{w}}}{1-S_{\mathrm{orw}}-S_{\mathrm{wirr}}}\right)^2 = (1-S_{\mathrm{w}})^2 \\ k_{\mathrm{rw}} &= M\,\frac{\mu_{\mathrm{w}}}{\mu_{\mathrm{o}}}\left(\frac{S_{\mathrm{w}}-S_{\mathrm{wirr}}}{1-S_{\mathrm{orw}}-S_{\mathrm{wirr}}}\right)^2 = M\,\frac{\mu_{\mathrm{w}}}{\mu_{\mathrm{o}}}S_{\mathrm{w}}^2 \end{aligned} \tag{6}$$

The one-dimensional Buckley–Leverett solution consists of a frontal shock at saturation $S_{\mathrm{w}}^*=1/\sqrt{M+1}$ and a rarefaction from that saturation to the injection saturation, $S_{\mathrm{w}}=1$. The mobility contrast at the front is given by $M^*=2(1-1/\sqrt{M+1})$. Once capillarity is introduced we will use the usual J-function scaling for the capillary pressure function. A logarithmic function of saturation will be used for the J-function itself.

$$\begin{aligned} P_{\mathrm{o}}-P_{\mathrm{w}}=P_{\mathrm{c}}(\mathbf{x},S_{\mathrm{w}}) &= \sigma\sqrt{\frac{\phi}{k}}\,J(S_{\mathrm{w}}) \\ J(S_{\mathrm{w}}) \sim -\ln\left(\frac{S_{\mathrm{w}}-S_{\mathrm{wirr}}}{1-S_{\mathrm{orw}}-S_{\mathrm{wirr}}}\right) &= -\ln(S_{\mathrm{w}}) \end{aligned} \tag{7}$$

This function has the appropriate scaling at the irreducible water saturation: $P_{\mathrm{c}}\to+\infty$ as $k_{\mathrm{rw}}\to 0$, and has vanishing entry pressure at the residual oil saturation: $P_{\mathrm{c}}=0$ at $S_{\mathrm{w}}=1$.

These equations are sufficiently rich to introduce the time of flight formulation. Consider an incompressible, steady state velocity field, $\mathbf{u}(\mathbf{x})$. Based upon this velocity, we will introduce three new co-ordinates, and transform the conservation equation accordingly. Two of the new co-ordinates are the bi-streamfunctions [18]. Because the flow is incompressible, it can be represented as the cross-product of these functions.

$$\mathbf{u}=\nabla\psi\times\nabla\chi \tag{8}$$

For instance, for two-dimensional incompressible flow, $\chi=z$ and $\psi=\psi(x,y)$ is the usual streamfunction. The third co-ordinate is the time of flight, $\tau(\mathbf{x})$, defined by integrating the transit time of a test particle moving at the interstitial velocity $\mathbf{u}/\phi$ backwards from $\mathbf{x}$ along its streamline (in three dimensions) to either an injection well or to a boundary.

$$\tau=\int_{\psi}\frac{\phi}{u}\,\mathrm{d}s \tag{9}$$

In differential form

$$\mathbf{u}\cdot\nabla\tau=\phi \tag{10}$$

The time of flight has units of time, but in fact it functions as a distance, which increases along a streamline. The bi-streamfunctions function as transverse co-ordinates. Figure 3 shows two different permeability fields and the resulting streamline patterns for flow from left to right in the rectangular domain. With small heterogeneity (low correlation or low variance) the time of flight and bi-streamfunction co-ordinates are essentially (x,y,z). As the permeability correlation increases, the time of flight and bi-streamfunction co-ordinates depart significantly from this simple rescaling of co-ordinates. Although this conceptualization invokes a single

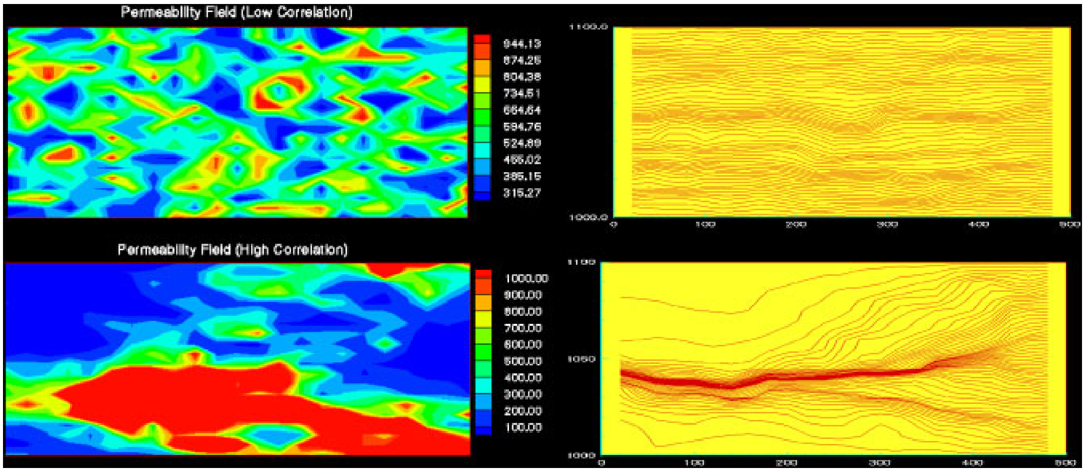

Figure 3. Permeability and streamlines (low and high permeability heterogeneity).

velocity field and particles, the time of flight formulation is not a particle tracker, nor is it restricted to single-phase flow.

The representation of Equation (1) requires the evaluation of the gradient operator.

$$\nabla = (\nabla\tau)\frac{\partial}{\partial\tau} + (\nabla\psi)\frac{\partial}{\partial\psi} + (\nabla\chi)\frac{\partial}{\partial\chi} \tag{11}$$

Or simply

$$\mathbf{u}\cdot\nabla = \phi\,\frac{\partial}{\partial\tau} \tag{12}$$

The differential equation is now apparently one-dimensional.

$$\frac{\partial S_{\mathrm{w}}}{\partial t} + \frac{\partial F_{\mathrm{w}}}{\partial\tau} = 0 \tag{13}$$

As already discussed, this transport equation may be solved numerically along each streamline. Or, if analytic techniques are used, then even more rapid fast performance estimations or up-scaling calculations may be performed, including the effects of an arbitrary three-dimensional heterogeneity field. The volume element also takes a simple form under this transformation:

$$\left\|\frac{\partial(\tau,\psi,\chi)}{\partial(x,y,z)}\right\| = \nabla\tau\cdot\nabla\psi\times\nabla\chi = \phi$$

$$\phi\,\mathrm{d}x\,\mathrm{d}y\,\mathrm{d}z = \mathrm{d}\tau\,\mathrm{d}\psi\,\mathrm{d}\chi = \mathrm{d}\tau\,\mathrm{d}q \tag{14}$$

In other words, the differential volume $\mathrm{d}\tau\,\mathrm{d}q$ along a streamline is equal to the pore volume in the original space. There is no requirement that each streamline be generated with identical fluxes, $\mathrm{d}q$. Correspondingly, this identity is important when re-sampling saturations from lines to the underlying grid. When incorrectly weighted, you may obtain the large mass balance errors alluded to earlier.

The time of flight derivations can be extended to compressible flows. In this case, the restriction on velocity, Equations (2) and (8), and the Jacobian of the volumetric transformation, Equation (14) will each be generalized. However, the primary definition of the time of flight, Equations (9) and (10), remain unchanged. To focus our attention on numerical stability, we will not include the physical mechanisms of compressibility in the current study.

This completes the presentation of the time of flight formulation for streamlines. A velocity field is used to generate a co-ordinate transformation in which the transport equation and the differential volume elements are simple to evaluate. Fortunately, the transverse co-ordinates ψ and χ do not enter into the resulting equations, as they are difficult to calculate. Only the time of flight co-ordinate τ and the volumetric flux $\mathrm{d}q$ enter into the equations, and both are easy to evaluate.

3. TRANSVERSE FLUX AND UNSTEADY STATE EFFECTS

The elegance of the streamline time of flight formulation is apparent in Equation (13). When we implement the numerical solution along streamlines for Equation (10), we have done so as a sequence of steady state approximations, just as we do in an IMPES formulation in a finite difference simulator. Unfortunately, unlike a traditional IMPES solution, the time step is now much larger, and the approximation that the total fluid velocity may be treated as constant during a time step cannot be as accurate. To understand the nature of this approximation, we now distinguish between the initial velocity, $\mathbf{u}_0$, and the instantaneous velocity, $\mathbf{u}$, during a time step. We define the time of flight co-ordinates, (τ, ψ, χ) using the initial velocity of the time step.

$$\mathbf{u}_0 \cdot \nabla\tau = \phi \tag{15}$$

The spatial derivative can now be written as its initial approximation, and a correction.

$$\begin{aligned} \mathbf{u} \cdot \nabla F_{\mathrm{w}} &= \mathbf{u}_0 \cdot \nabla F_{\mathrm{w}} + (\mathbf{u} - \mathbf{u}_0) \cdot \nabla F_{\mathrm{w}} \\ &= \phi \frac{\partial F_{\mathrm{w}}}{\partial \tau} + (\mathbf{u} - \mathbf{u}_0) \cdot \nabla F_{\mathrm{w}} \end{aligned} \tag{16}$$

The second term in Equation (16) represents the transverse flux because of changes in instantaneous velocity. As in much of the streamline literature, these equations are solved using operator splitting. A time step consists of a longitudinal convective step, followed by the transverse flux step: $\partial S_{\mathrm{w}}/\partial t \rightarrow \partial S_{\mathrm{w}}/\partial t_1 + \partial S_{\mathrm{w}}/\partial t_2$. Equation (1) now becomes

$$\phi \frac{\partial S_{\mathrm{w}}}{\partial t_1} + \phi \frac{\partial S_{\mathrm{w}}}{\partial t_2} + \phi \frac{\partial F_{\mathrm{w}}}{\partial \tau} + (\mathbf{u} - \mathbf{u}_0) \cdot \nabla F_{\mathrm{w}} = 0 \tag{17}$$

which may be grouped and split into the following two equations.

$$\frac{\partial S_{\mathrm{w}}}{\partial t_1} + \frac{\partial F_{\mathrm{w}}}{\partial \tau} = 0 \tag{18}$$

$$\phi \frac{\partial S_{\mathrm{w}}}{\partial t_2} + (\mathbf{u} - \mathbf{u}_0) \cdot \nabla F_{\mathrm{w}} = 0 \tag{19}$$

To within the operator splitting approximation, this pair of equations is equivalent to the original three-dimensional flow equation. The first equation, Equation (18) is identical to the usual streamline equation, Equation (13). It may be solved using the techniques already in place within a streamline simulator. The second equation, Equation (19) is identical to our usual conservation equation, Equation (1), but with the velocity replaced by an unsteady state velocity. It includes any and all unsteady state effects, whether transverse or longitudinal. It may be solved using any of the techniques applied within conventional finite difference simulation. These equations combine to provide a 'predictor–corrector' formulation. Numerical predictor–corrector strategies are effective if the predictor provides a good first approximation, and if the corrector is relative small. Because of the quality of the streamline approximation, we will satisfy this requirement. What have we achieved? As an industry, we have a great deal of expertise in solving each of these equations. Now we recognize that rigorous streamline simulation relies on solving these two equations in a coupled fashion.

How well does this correction work? We have examined waterflood in a simple geometry—the quarter five spot, with fixed and equal injection and production rates. This is the simplest possible model that will show the effects of viscous cross-flow. To study the cross-flow we vary:

(a) Mobility ratios of $M = 0.2, 0.5, 0.9, 10.0$ ($M^* = 0.17, 0.37, 0.55, 1.4$).
(b) Time steps of $\Delta t = 10$ days, 20 days, 60 days (0.011, 0.022, 0.066 pore volumes injected).
(c) Permeability either homogeneous or heterogeneous.

Porosity is constant and not varied. The simulation is done on a 21×21 cell grid. Varying the mobility ratio will modify the amount of cross-flow in the system. Varying the time step size will change the quality of the piecewise steady state approximation for the flow field—larger time steps will have fewer velocity re-calculations and larger cross-flow.

In Figure 4 we show the results of the simulation at 0.4 PVI, for $M = 0.2$, for the three different time steps. We also show the saturation correction after the first time step for the largest and smallest time step sizes. As expected, the cross-flow corrections occur at the flood front. The sign of the saturation correction corresponds to flood stabilization: the front slows down and the profile will broaden. For the largest time step, the cross-flow correction is not sufficient to reduce the speed of the front. In all cases the cross-flow correction only has a local impact on the solution. A finite difference simulation is included as a reference.

The solution is displayed as a function of time in Figure 5, where we plot water-cut. In this case we report the results for the extremes of mobility ratio and for the minimum and maximum time step size. We also include the results with and without the cross-flow correction. Again, a finite difference simulation is included as a reference. In Figure 5 we see two effects. First, the saturation corrections are negligible in terms of the water-cut development—the saturation cross-flow does not change the large scale behaviour of the solution. More importantly, however, are the oscillations which have become apparent in the solutions as the amount of cross-flow increases. For the highest mobility ratio, small oscillations in the profile are only seen at the largest time step. For the lowest mobility ratio, oscillations are much more apparent, and occur at both the 20 day and the 60 day time steps.

All the cases simulated are summarized in Table I. The values in the table are the maximum saturation correction at the first time step. The cells in the table are colour coded according to the stability of the solution. If any oscillations are seen in the water-cut curve, then the cells

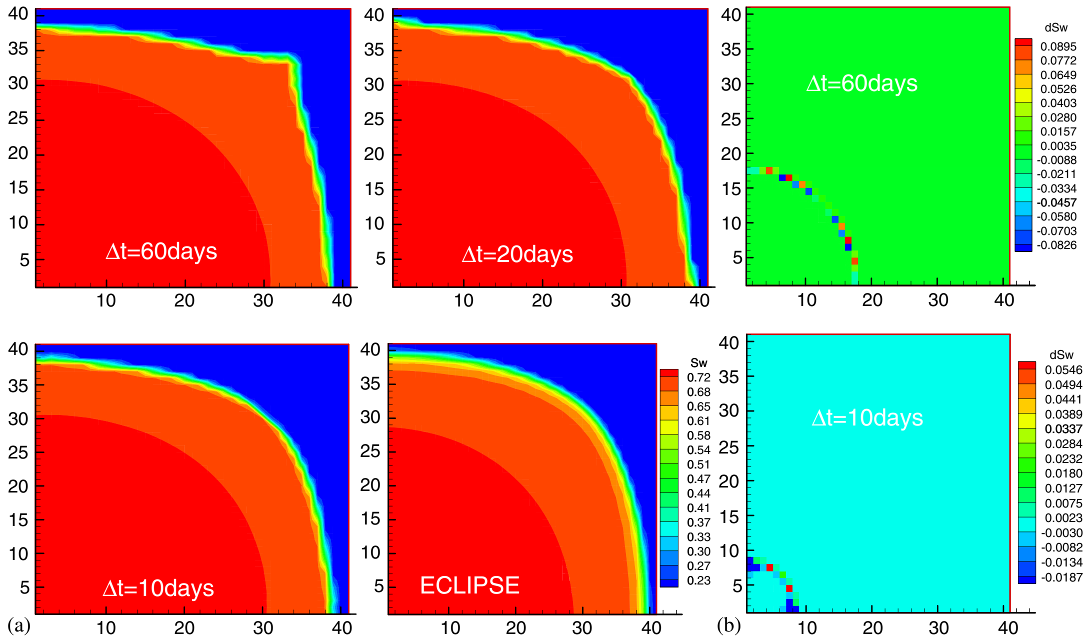

Figure 4. (a) Saturations at 0.4 PVI for $\Delta t = 10$ days, 20 days, 60 days and ECLIPSE. (b) Saturation corrections after one time step for $\Delta t = 10$ days and 60 days.

are shaded. There is no obvious correlation between the limit of stability and the magnitude of the saturation correction.

4. TIME STEP CONTROL VIA A TRANSVERSE CFL CONSTRUCTION

What is missing from the above analysis? What can provide us with guidance on the nature of the oscillations seen in the water-cut development? We know that the instability becomes more apparent as the cross-flow, $(\mathbf{u} - \mathbf{u}_0)$ increases, and also as the time step size increases. For a one-dimensional Buckley–Leverett waterflood solution, stability of an IMPES numerical scheme is governed by the CFL number [19].

$$\mathrm{CFL} = \frac{u}{\phi} \frac{\Delta t}{\Delta x} F'_{\mathrm{w}} \tag{20}$$

The limit of stability, $\mathrm{CFL} = 1$, determines the maximum stable time step size. At this time step, the wave with maximum speed will cross one cell (Δx). A corresponding construction for the CFL number in three dimensions is known [20]. Working with cell volumes and volumetric flux instead of distances and velocities, we can construct the following discrete CFL number,

$$\mathrm{CFL} = \frac{\Delta t}{PV} \sum_{\text{Inflow Faces}} \left(\mathbf{u}_{\mathrm{f}} \cdot \mathbf{n}_{\mathrm{f}} \cdot \operatorname*{Max}_{S_{\mathrm{wf}}} \left(\frac{[F_{\mathrm{w}}]}{[S_{\mathrm{w}}]} \right) \right) \tag{21}$$

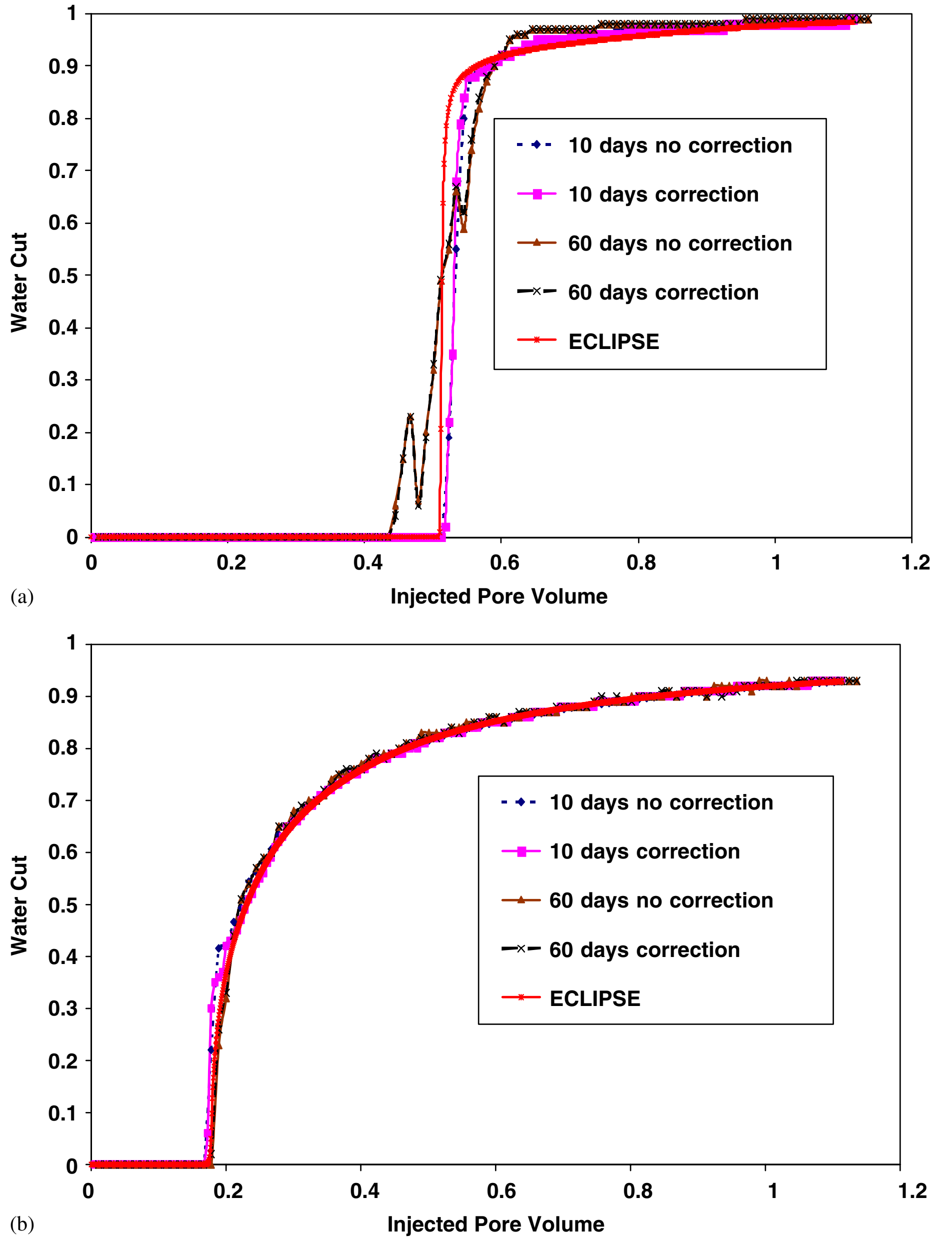

Figure 5. Water-cut for the homogeneous quarter five spot (a) $M = 0.2$; and (b) $M = 10.0$.

The summation is only taken over the inflow faces, e.g. $\mathbf{n}_f$ is inwardly directed cell face area, and $\mathbf{u}_f \cdot \mathbf{n}_f$ must be positive. This is consistent with the interpretation of the CFL number as being dependent upon the fastest wave which moves across a cell.

Table I. Maximum saturation correction for all cases. Shaded cells show oscillatory water-cut development.

ΔS_wMax		Time step (days) 10	20	60
Homogeneous	$M = 0.2$	0.0598	0.0419	0.1017
	$M = 0.5$	0.022	0.0894	0.0838
	$M = 0.9$	0.0147	0.0395	0.0765
	$M = 10$	0.0231	0.0209	0.0612
Heterogeneous	$M = 0.2$	0.0472	0.0914	0.1183
	$M = 0.5$	0.0742	0.0757	0.0949
	$M = 0.9$	0.0352	0.0309	0.0840
	$M = 10$	0.0260	0.0372	0.0564

The only subtlety in this equation is in the discrete form of the wave speed. We can think of the saturation of the adjacent cell, $S_{\mathrm{w,Face}}$, flooding into the cell, $S_{\mathrm{w,Cell}}$, which will form a Buckley–Leverett profile. Whether we have a pure rarefaction, a shock, or a contact discontinuity depends upon the specific saturations and the fractional flow function. The wave speed that contributes to the CFL restriction is the fastest wave. Specifically, if we consider all saturations S_{w} intermediate between $S_{\mathrm{w,Face}}$ and $S_{\mathrm{w,Cell}}$, then the speed is the maximum of $(F_{\mathrm{w}}(S_{\mathrm{w}}) - F_{\mathrm{w}}(S_{\mathrm{w,Cell}}))/(S_{\mathrm{w}} - S_{\mathrm{w,Cell}})$. If there is no saturation contrast across a face, then this wave speed is set to zero, as there is no contribution to the evolution equation. This form of the discrete CFL number fully accounts for both saturation discontinuities and flow direction reversals. It will also account for the more general form of the fractional flow function that includes the effects of gravity.

Equation (21) is the CFL construction for the Buckley–Leverett equation in three dimensions, Equation (1). There is no obvious time step limitation in Equation (18). This leaves only Equation (19), which is of the same form as Equation (1) but with the transverse velocity, $\mathbf{u} - \mathbf{u}_0$ instead of $\mathbf{u}$.

$$\Delta\mathrm{CFL} = \frac{\Delta t}{PV} \sum_{\text{Inflow Faces}} \left((\mathbf{u}_{\mathrm{f}} - \mathbf{u}_0) \cdot \mathbf{n}_{\mathrm{f}} \cdot \operatorname*{Max}_{S_{\mathrm{wf}}} \left(\frac{[F_{\mathrm{w}}]}{[S_{\mathrm{w}}]} \right) \right) \tag{22}$$

We use the symbol ΔCFL to distinguish from the CFL for Equation (1). We repeat the data presentation of Table II, but now we calculate the maximum ΔCFL instead of the maximum saturation change. The limit of stability is clearly equal to $\Delta\mathrm{CFL} = 1$. At this time step size, the transverse flux is sufficient to shift a streamline laterally by one cell. Beyond this time step, the streamlines are sufficiently out of alignment with the saturations, that we no longer have monotonic saturation profiles along individual streamlines. This is shown clearly in Figure 6 which shows a detailed view near the outlet of the system for $M = 0.2$, 60 day time steps, at 0.4 PVI.

We contrast the CFL number of the original equation and the correction CFL in Figure 7. We see approximately a ten-fold reduction in the effective CFL number by using the streamline predictor step as a pre-conditioner. This is very reasonable for a problem with strong cross-flow. For less severe cross-flow, the value of $\mathbf{u} - \mathbf{u}_0$ can become quite small, giving even greater benefits for streamline simulation. These trends are completely consistent

Table II. Maximum correction CFL for all cases. Shaded cells show oscillatory water-cut development.

Correction CFL		Time step (days)		
		10	20	60
Homogeneous	$M=0.2$	0.513	1.218	2.343
	$M=0.5$	0.567	0.716	1.385
	$M=0.9$	0.298	0.468	1.47
	$M=10$	0.488	0.649	2.306
Heterogeneous	$M=0.2$	1.166	1.73	3.755
	$M=0.5$	0.884	1.362	2.679
	$M=0.9$	0.689	1.006	1.794
	$M=10$	0.705	0.954	1.59

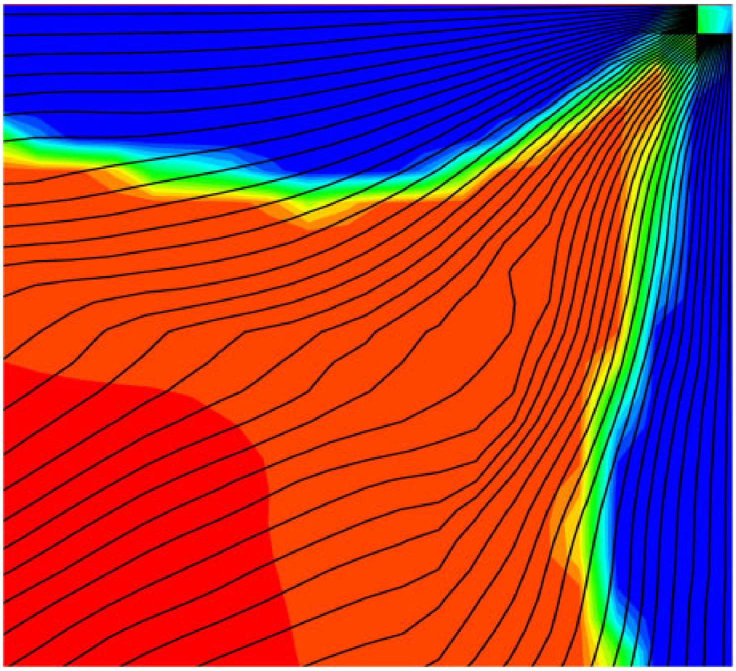

Figure 6. Streamlines and saturations for $M=0.2$, 0.4 PVI, 60 day time steps, heterogeneous permeability. The image has been zoomed in to the vicinity of the outlet.

with the industry's empirical experience with streamline time step control. For the first time, we now have the ability to predict the maximum allowable time step size for a streamline simulation. It is interesting to note that this limit occurs irrespective of the means used to solve the saturation correction equation. Even if a fully implicit technique was used to solve Equation (19), the streamline predictor construction is essentially IMPES.

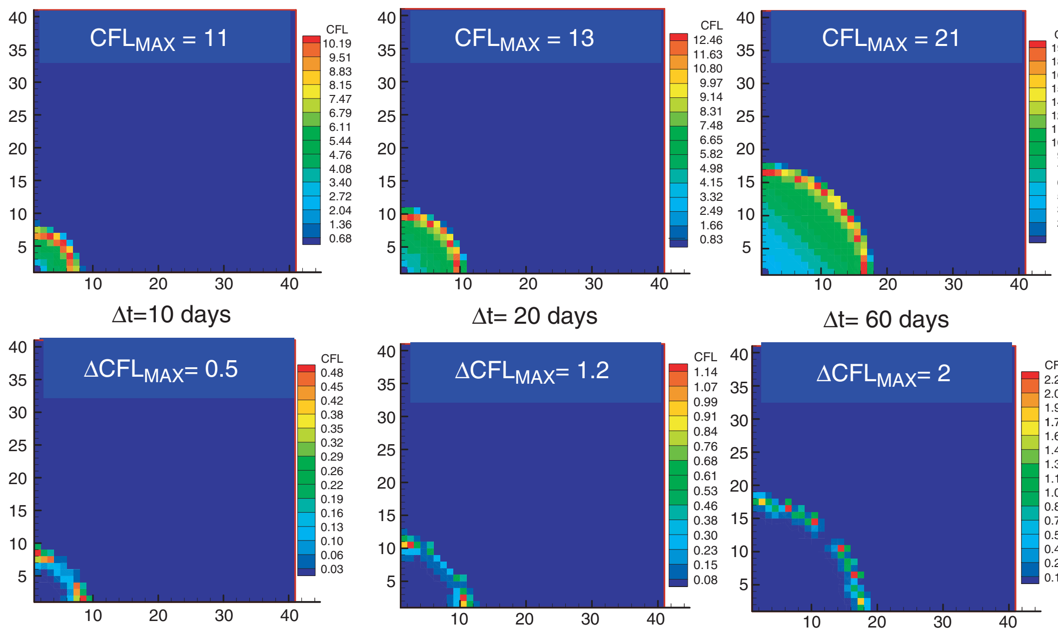

Figure 7. CFL and correction CFL after the first time step for $M = 0.2$, homogeneous permeability.

5. TREATMENT OF GRAVITY AND CAPILLARITY

What about other physical effects? We now extend the discussion to cover the effects of gravity and of capillarity [21–25]. The water phase velocity $\mathbf{u}F_{\mathrm{w}}$ is replaced by a more complete expression.

$$\mathbf{u}_{\mathrm{w}} = \frac{\lambda_{\mathrm{w}}}{\lambda_{\mathrm{t}}}\mathbf{u} + \frac{\lambda_{\mathrm{w}}\lambda_{\mathrm{o}}}{\lambda_{\mathrm{t}}}\nabla(P_{\mathrm{c}} - \Delta\rho g z) \tag{23}$$

The total velocity is also modified.

$$\mathbf{u} = -\lambda_{\mathrm{t}}\nabla(P_{\mathrm{w}} + \rho_{\mathrm{w}} g z) - \lambda_{\mathrm{o}}\nabla(P_{\mathrm{c}} - \Delta\rho g z) \tag{24}$$

We can define the fractional flow of water, f_{w}, (for non-zero total velocity) by projecting the water flux in the direction of the total velocity.

$$u^2 f_{\mathrm{w}} \equiv \mathbf{u}\cdot\mathbf{u}_{\mathrm{w}} = \frac{\lambda_{\mathrm{w}}}{\lambda_{\mathrm{t}}}u^2 + \frac{\lambda_{\mathrm{w}}\lambda_{\mathrm{o}}}{\lambda_{\mathrm{t}}}\mathbf{u}\cdot\nabla(P_{\mathrm{c}} - \Delta\rho g z) \tag{25}$$

Here $\Delta\rho = \rho_{\mathrm{w}} - \rho_{\mathrm{o}}$ is the density difference between the phases, and the capillary pressure was defined earlier, Equation (7). For the one-dimensional example calculations, we will use quadratic relative permeabilities and logarithmic capillary pressure. The fractional flow function can then be written as

$$f_w = F_w(S_w) - \alpha G(S_w) - \beta H(S_w)\frac{\partial S_w}{\partial x}$$

$$G(S_w) = \frac{MS_w^2(1-S_w)^2}{MS_w^2 + (1-S_w)^2} \tag{26}$$

$$H(S_w) = \frac{MS_w(1-S_w)^2}{MS_w^2 + (1-S_w)^2}$$

The examples will use $M = 3$, $\alpha = 20$, and $\beta = 0.1$.

Let us first consider the effects of gravity. It has been widely implemented using operator splitting within various streamline simulators. We will see that its implementation raises no particular issues. We split the time step into a convective time step and a gravity time step. First we have a 'predictor' convective step and use $f_w = F_w(S_w)$. In the gravity 'corrector' step, $f_w = -\alpha G(S_w)$. This is no longer a transverse flux correction—it is a representation of the vertical segregation of fluids due to gravity. We solve the gravity step with an explicit numerical scheme, and try three different time step sizes, Figure 8. This equation has its own CFL construction, which follows from Equation (21). If we use an explicit solution for the gravity, and if we exceed the limit of CFL = 1, then the solution is unstable. In this particular instance, we can either cut the time step to satisfy CFL < 1 or we can choose to use an implicit technique. The finite difference solution is included for reference, and we see that the gravity operator splitting has worked perfectly.

Let us now look at the effects of capillarity. Figure 9 shows the fractional flow curve with its concave envelope. In the absence of capillarity, the analytic solution satisfies an entropy condition and follows the concave envelope. A singular perturbation analysis can be used to demonstrate that the effect of capillarity on the fractional flow is identical—again, the solution follows the concave envelope [21]. The effect of capillarity on the saturation profile is that the saturation shock spreads to a finite width which depends upon the strength of capillarity relative to the viscous pressure drop. But otherwise, the solution with capillarity is very similar to the solution without capillarity. Figure 9(a) replicates the solution in Figure 8 without gravity, to within the effects of numerical dispersion. Similarly, Figure 9(b) replicates the full finite difference solution.

What happens when we split capillarity from the fractional flow in the natural way: $f_w = F_w(S_w)$ followed by $f_w = -\beta H(S_w)\partial S_w/\partial x$? The results are shown in Figure 10. Unlike the case of gravity, the operator split solution does not converge to the finite difference solution—it is too diffusive. This effect has been described before, e.g. References [22–24]. The residual between the concave envelope and the fractional flow acts as an anti-diffusive term which must be included in the operator splitting: $f_w = \tilde{F}_w(S_w)$ and $f_w = F_w(S_w) - \tilde{F}_w(S_w) - \beta H(S_w)\partial S_w/\partial x$. Figure 10(b) shows that this split successfully converges. The only solution which does not require this correction to the operator splitting is obtained if the original convective step is reduced to very small time steps [22, 25]. Of course, this defeats the intent of streamline simulation.

The capillary equation is now a non-linear diffusion problem. The equivalent of the CFL number and the limit CFL = 1 is the diffusion number, $\mathrm{DN} = -\beta H(S_w)\Delta t/\Delta x^2$ and the limit

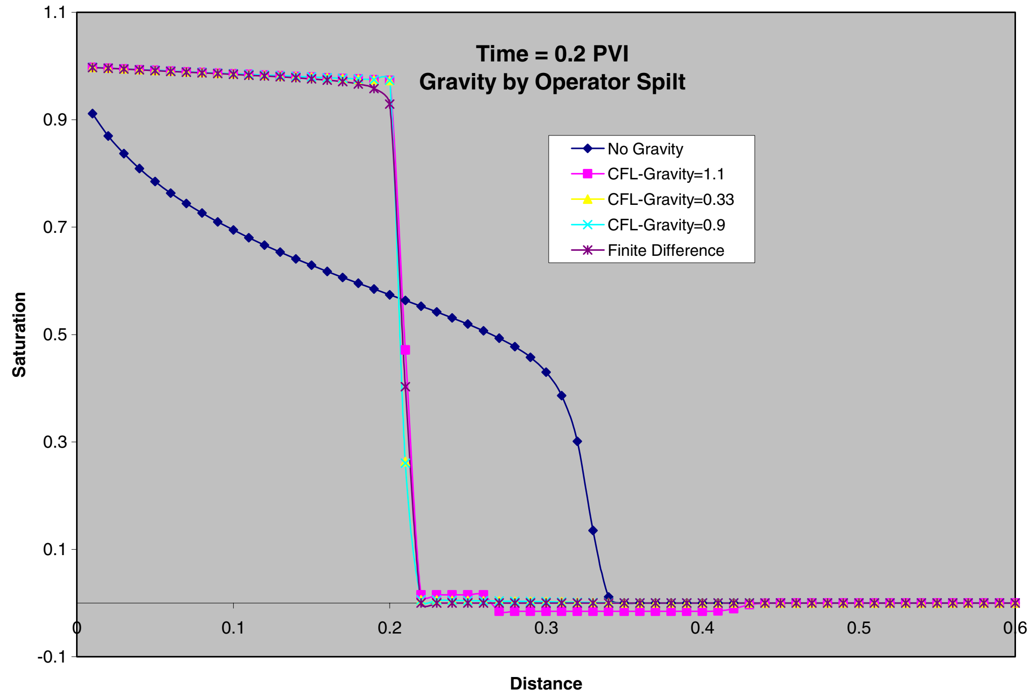

Figure 8. Saturation profile with gravity. (a) No gravity; (b) gravity, CFL = 1.1; (c) gravity, CFL = 0.33; (d) gravity, CFL = 0.9; and (e) finite difference.

DN $= \frac{1}{2}$ for an IMPES calculation. Again, this is probably best solved using an implicit technique. Figures 10(a) and (b) both show very strong instabilities once this stability limit is exceeded.

Although this anti-diffusive correction appears to provide a successful treatment of capillarity, consider how it needs to be applied in practice in three dimensions. The shape of the fractional flow curve will vary tremendously throughout the model as velocities and dips vary. Examine the difference between Figure 9(a) and (b); you obtain completely different concave envelopes and residual corrections. As discussed in Reference [22], failure to get an accurate residual will generate spurious results. A simpler treatment is to split the water flux into its longitudinal and transverse components. The longitudinal flux was defined in Equation (25)

$$\mathbf{u}_{\mathrm{w}} = \mathbf{u} f_{\mathrm{w}},\ f_{\mathrm{w}} \equiv \frac{\mathbf{u}\cdot\mathbf{u}_{\mathrm{w}}}{u^2} = \frac{\lambda_{\mathrm{w}}}{\lambda_{\mathrm{t}}} + \phi\,\frac{\lambda_{\mathrm{w}}\lambda_{\mathrm{o}}}{u^2\lambda_{\mathrm{t}}}\,\frac{\partial}{\partial\tau}(P_{\mathrm{c}} - \Delta\rho g z)$$

The remaining transverse flux is obtained from the orthogonal projection operator $(\overleftrightarrow{1} - \mathbf{uu}/u^2)\cdot\mathbf{u}_{\mathrm{w}} = \lambda_{\mathrm{w}}\lambda_{\mathrm{o}}/\lambda_{\mathrm{t}}(\overleftrightarrow{1} - \mathbf{uu}/u^2)\cdot\nabla(P_{\mathrm{c}} - \Delta\rho g z)$. This reduces to the un-split solution in one dimension, and no longer has need of a concave envelope construction for the second equation. It should be noted that in the recent work of Berenblyum *et al.* [25], that transverse capillary flux is very strong, and we will obtain essentially the same results. However, in the longitudinal direction we do not require the anti-diffusive corrections utilized in References [22–24].

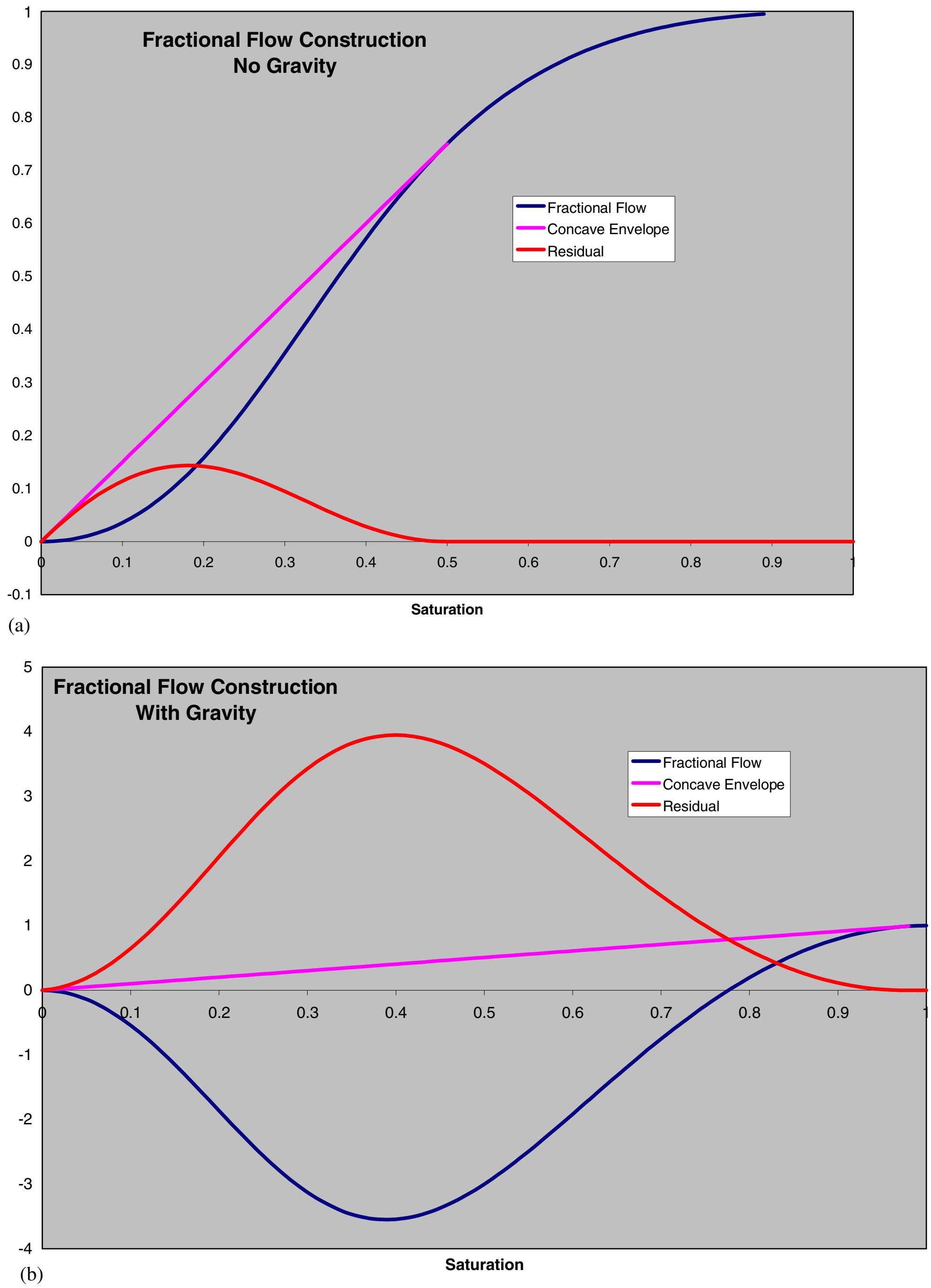

Figure 9. Fractional flow construction. (a) No gravity; and (b) with gravity.

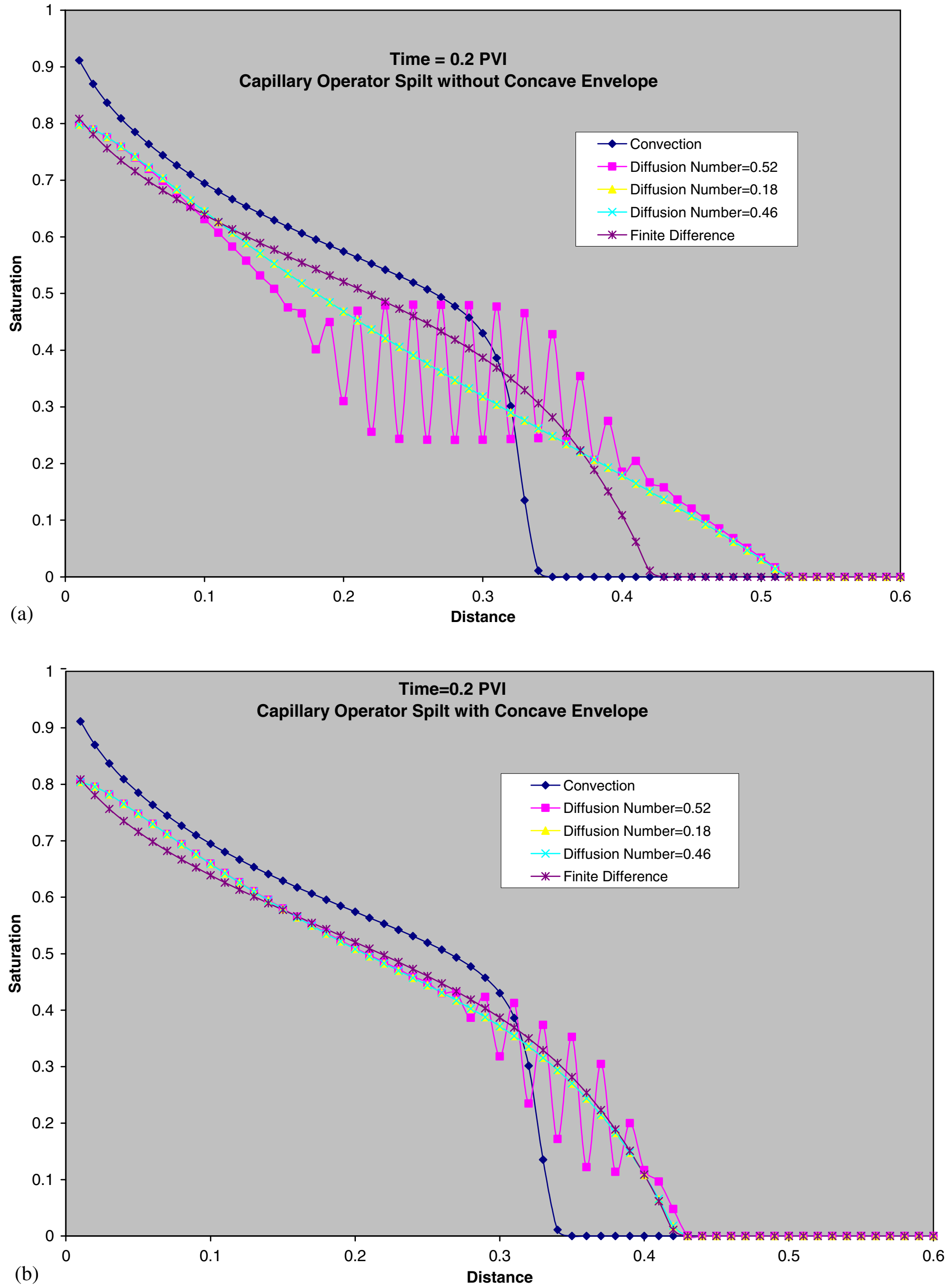

Figure 10. Saturation profile with capillarity. (a) Without concave envelope correction; and (b) with concave envelope correction. Each plot has five curves: (1) No capillarity, (2) capillarity, DN = 0.52, (3) capillarity, DN = 0.18, (4) capillarity, DN = 0.46, (5) finite difference.

6. CONCLUDING DISCUSSION

There is one theme in this discussion: the stability of streamline simulation can be assessed by the same techniques that have been applied to conventional finite difference calculations. This provides a level of rigor that has been un-recognized to date. The transverse flux corrections allow us to understand the impact of unsteady state velocity. The operator split treatment for gravity seems to hold no issues. However, capillarity needs to be managed with some care. A specific split construction for capillarity, which will side-step the known issues, has been proposed.

Numerical stability is necessary, but not sufficient, for a numerical method. The current work provides a theoretical and practical solution to the question of stability. The study of convergence, and accuracy of the solution remains open questions for streamline simulation.

REFERENCES

1. Osako I, Datta-Gupta A, King MJ. Timestep selection during streamline simulation via transverse flux correction. *SPE 79688, presented at the SPE Reservoir Simulation Symposium*, Houston, TX, 3–5 February 2003.
2. Bratvedt F, Bratvedt K, Buchholz CF, Gimse T, Holden H, Holden L, Risebro NH. FRONTLINE and FRONTSIM. Two full scale, two-phase, black oil reservoir simulators based on front tracking. *Survey on Mathematics in Industry* 1993; **3**:185.
3. Bratvedt F, Bratvedt K, Buchholz CF, Holden L, Holden H, Risebro NH. A new front tracking method for reservoir simulation. *SPE Reservoir Engineering* 1992; **7**:107.
4. King MJ, Blunt M, Mansfield M, Christie MA. Rapid evaluation of the impact of heterogeneity on miscible gas injection. *SPE 26079 Presented at the SPE Western Regional Meeting (1993)*. In *New Developments in Improved Oil Recovery*, De Haan HJ (ed.). Geological Society Special Publication 84. Bath: U.K., 1995.
5. Thiele M, Blunt MJ, Orr FM. A new technique for predicting flow in heterogeneous systems using streamtubes. *Paper SPE/DOE 27834 Proceedings of the 9th Symposium on Improved Oil Recovery*, Tulsa, OK, April 1994.
6. Datta-Gupta A, King MJ. A semianalytic approach to tracer flow modeling in heterogeneous permeable media. *Advances in Water Resources* 1995; **18**(1):9.
7. Bratvedt F, Gimse T, Tegnander C. Streamline computations for porous media flow including gravity. *Transport in Porous Media* 1996; **25**:63.
8. Batycky RP, Blunt MJ, Thiele MR. A 3D field scale streamline-based reservoir simulator. *SPE Reservoir Engineering* 1997; **12**:246.
9. King MJ, Datta-Gupta A. Streamline simulation: a current perspective. *In Situ* 1998; **22**(1):91–140.
10. Crane MJ, Blunt MJ. Streamline-based simulation of solute transport. *Water Resources Research* 1999; **35**(10): 3061–3078.
11. Jessen K, Orr FM. Compositional streamline simulation. *SPE 77379 Presented at the SPE Annual Technical Conference and Exhibition*, San Antonio, TX, 29 September–2 October 2002.
12. Risebro NH, Tveito A. A front-tracking method for conservation laws in one dimension. *Journal of Computational Physics* 1992; **101**(1):130–139.
13. Ponting DK. Hybrid streamline methods. *SPE 39756 Presented at the 1998 Asia Pacific Conference on Integrated Modeling*, Kuala Lumpur, Malaysia, 23–24 March 1998.
14. Pollock DW. Semianalytical computation of path lines for finite–difference models. *Ground Water* 1998; **26**(6).
15. Datta-Gupta A, Lake LW, Pope GA, King MJ. A type-curve approach to analyzing two-well tracer tests. *SPE 24139 Presented at the SPE/DOE Symposium on EOR*, Tulsa, OK, 1992 (Also, SPE Form. Eval., 10, 40 (1995)).
16. Cordes C, Kinzelbach W. Continuous groundwater velocity fields and path lines in linear, bilinear, and trilinear finite elements. *Water Resources Research* 1992; **28**(11):2903–2911.
17. Prevost M, Edwards MG, Blunt MJ. Streamline tracing on curvilinear structured and unstructured grids. *SPE 78663*, SPEJ, June 2002.
18. Bear J. *Dynamics of Fluid in Porous Media*. Dover Publications: New York, 1973.
19. Trangenstein JA. *Numerical Analysis of Reservoir Fluid Flow*, *Multiphase Flow in Porous Media*: *Mechanics, Mathematics and Numerics*, Lecture Notes in Engineering, vol. 34. Springer: Berlin, 87–246.
20. Spivak A, Coats KH. Numerical simulation of coning using implicit production terms. *SPE Journal* 1970; 257–267.

21. King MJ, Dunayevsky VA. Why waterflood works—a linearized stability analysis. *SPE 19648 Proceedings of the SPE ATCE*, Las Vegas, NV, October 1989.
22. Karlsen KH, Brusdal K, Dahle HK, Evje S, Lie K-A. The corrected operator splitting approach applied to a nonlinear advection-diffusion problem. *Computer Methods in Applied Mechanics and Engineering* 1998; **167**:239–260.
23. Espedal MS, Karlsen KH. Numerical solution of reservoir flow models based on large time step operator splitting algorithms. *Filtration in Porous Media and Industrial Applications* (Cetraro, Italy 1998), Lecture Notes in Mathematics, vol. 1734. Springer: Berlin, 2000.
24. Rodruiguez PG, Segura MK, Mustieles Moreno FJ. Streamline methodology using an efficient operator splitting for accurate modeling of capillary and gravity effects. *SPE 79693 Proceedings of the SPE Reservoir Simulation Symposium*, Houston, TX, February 2003.
25. Berenblyum RA, Shapiro AA, Jessen K, Stenby EH, Orr FM. Black oil streamline simulator with capillary effects. *SPE 84037 Proceedings of the SPE ATCE*, Denver, CO, October 2003.
26. Datta-Gupta A. Accurate resolution of physical dispersion in the multidimensional numerical modeling of miscible and chemical displacement. *SPE 17338*, *SPE Reservoir Engineering* 1990; **15**(4):581–588.

